Detection of Spherical Inclusions Using Active Surfaces

Daniel A. Cook, Francesco Fedele, and Anthony J. Yezzi

***Abstract*—This paper addresses the problem of detecting and visualizing objects embedded within a surrounding medium. A new approach is outlined in which the ultimate goal is to directly reconstruct the shape of an inhomogeneity using active surfaces, which are multidimensional geometric entities that can be evolved iteratively until the minimum of a specified energy functional is reached. The surface is developed from an energy to be minimized, such that driving the active surface to match the shape of the inclusion reduces a chosen energy functional capturing the degree of mismatch between the true and estimated surfaces. Applications for this technique range from imaging objects in the ocean to visualizing tumors in the human body.**

***Index Terms*—Active surfaces, adjoint methods, buried objects**

I. Introduction

Traditional imaging techniques like synthetic aperture sonar make often-accurate, but very restrictive, simplifications about the scattered energy received by the sensor. Specifically, one of the standard assumptions is that waves propagate in a free space that is homogeneous, except for a distribution of infinitesimally-small point scatterers that do not interact with each other. This solution is otherwise known as the free-space Green's function: the ubiquitous $\exp\{ikR\}/R$ term that serves as the basis for nearly all coherent sonar and radar processing. Decades of technology development attest to the fact that this model works well in many settings. Nevertheless, its limitations become clear in situations involving complicated effects such as multipath and sediment penetration.

This paper addresses the problem of detecting and visualizing buried objects. A new approach is outlined in which the objective is to directly reconstruct the shape of an inhomogeneity using active surfaces, as opposed to creating a conventional image of the environment. Active surfaces are multidimensional geometric entities that can be evolved iteratively until the minimum of a specified energy functional is reached [1]–[3]. The surface is related to an energy to be minimized, such that driving the active surface to match the shape of the inclusion reduces the chosen energy functional.

The energy minimized is the mismatch between the observed acoustic energy scattered by the object and that predicted from its estimated shape and position, represented by the active surface. In order to evolve the surface from one iteration to the next it is necessary to compute both the acoustic field and its gradient on the active surface.

Manuscript received July 30, 2010; revised August 9, 2010.

D. Cook is with the Sensors and Electromagnetic Applications Laboratory of the Georgia Tech Research Institute, Atlanta, GA. E-mail: dan.cook@gtri.gatech.edu

F. Fedele is with the School of Civil and Environmental Engineering of the Georgia Institute of Technology, Savannah, GA. E-mail: francesco.fedele@gtsav.gatech.edu

A. Yezzi is with the School of Electrical and Computer Engineering of the Georgia Institute of Technology, Atlanta, GA. E-mail: ayezzi@ece.gatech.edu

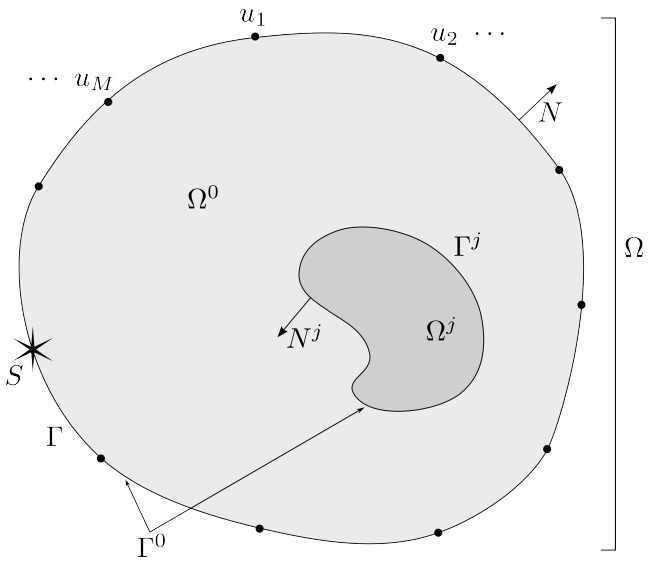

Fig. 1. Source illuminating a spherical flaw embedded in a domain containing several measurement locations. A single source is shown from clarity. The technique presented is equally valid for an arbitrary number of sources.

This work provides the theoretical foundation necessary for the ambitious goal of reconstructing the boundary of arbitrarily-shaped objects buried in the sea floor. The example results presented are limited in scope to spherical objects embedded in a homogeneous medium. A closed-form eigenexpansion in terms of spherical harmonics is used to compute the required field values along the active surface without having to resort to approximate methods.

II. Derivation of shape gradient

Consider, as shown in Fig. 1, the domain Ω partitioned as $\Omega = \Omega^0 \cup \Omega^j$, where the internal boundaries of the j subdomains are denoted Γ^j and the outer boundary as Γ. Thus, the outer domain (the one containing the subdomains, or 'inclusions') is denoted as Ω^0, its outer boundary is Γ, and its complete boundary is $\Gamma^0 = \Gamma \cup \Gamma^j$. Within the outer domain and the j^{th} subdomain, the material properties are homogeneous and characterized by the pairs (d^0, μ^0) and (d^j, μ^j) respectively.

The information of ultimate interest is an estimate of the boundaries Γ^j, which in the present example represent objects buried in the sea floor. We reach this objective by meeting a

secondary goal of reconstructing a function u over the domain Ω given a known excitation source S as well as a set of M measurements $\hat{u}_m = u(x_m) + \eta_m$ at different points $x_m \in \Gamma$, $m = 1, \ldots, M$, along the boundary, where η_m are random samples from a zero-mean measurement noise process η. The function u is governed by the following PDE and Robin boundary value constraint

$$\mathcal{L}u = S, \qquad x \in \Omega \tag{1a}$$

$$\frac{\partial u}{\partial N} + Bu = 0, \qquad x \in \Gamma. \tag{1b}$$

The operator $\mathcal{L}$ depends upon the partitioning Ω^j, $j = 0, \ldots, n$ of the domain Ω resulting from the unknown interior surfaces Γ^j, $i = 1, \ldots, n$ and is defined as follows

$$(\mathcal{L}u)(x) = (\mathcal{L}^j u^j)(x), \quad x \in \Omega^j \tag{2a}$$

with

$$\mathcal{L}^j \doteq -d^j \triangle + \mu^j, \quad (j = 0, \ldots, n), \tag{2b}$$

where u^j denotes the restriction of u to Ω^j with the following matching boundary conditions

$$u^0 = u^j \tag{2c}$$

and

$$d^0 \frac{\partial u^0}{\partial N^0} = -d^j \frac{\partial u^j}{\partial N^j}, \tag{2d}$$

for $x \in \Gamma^j$, $\quad (j = 1, \ldots, n)$ imposed across the internal contours Γ^j. The operator (2) describes the propagation of single-frequency waves, where $\mu = -k^2/d$, k is the wavenumber, and d is a diffusion coefficient. In typical acoustic applications where there is no diffusion ($d = -1$) and the wavenumber equals $2\pi/\lambda$, Equation (2) is the Helmholtz operator. If one wishes to account for attenuation due to absorption of acoustic energy, then the wavenumber is complex-valued, with the imaginary part representing the absorption term. In the event that the constant B in (1) equals zero, the Robin boundary condition collapses to a Neumann condition. For underwater acoustics this corresponds to a pressure-release surface such as an air-water interface, when u is taken to represent the sound pressure.

For the sake of convenience, we will let $d = (d^0, \ldots, d^n)$ and $\mu = (\mu^0, \ldots, \mu^n)$ denote the full set of d^j and μ^j coefficients respectively. No similar notation will be used for the set of interior boundaries Γ^j since we are already reserving the symbol Γ for the exterior boundary of the complete domain Ω. However, we can still denote the full set of Γ^j's compactly by noting that $\Gamma^1 \cup \ldots \cup \Gamma^n = \Gamma^0 \setminus \Gamma$. A condensed summary, therefore, is that the operator $\mathcal{L}$ in our forward model (1) is defined by (2) once d, μ, and $\Gamma^0 \setminus \Gamma$ are given.

A. Variational Formulation of Inverse Problem

We may now state the inverse problem as that of determining the unknown partition surfaces $\Gamma^0 \setminus \Gamma$ which produce an operator $\mathcal{L}$, via (2), that yields a function u whose values at each x_m match the known measurements $\hat{u}_m$ once the corresponding forward model (1) has been solved. It is assumed that the coefficients d and μ are known.

B. Energy to Minimize

Since the measurements are subject to noise, we may frame the desired matching problem in the least squares sense by choosing the surface $\Gamma^0 \setminus \Gamma$ to minimize the following energy terms representing the summed squared error:

$$E_M = \sum_{m=1}^{M} \frac{1}{2}\big(u(x_m) - \hat{u}_m\big)^2. \tag{3}$$

The energy E_M may also be written in integral form as

$$E_M = \int_\Gamma g\big(u(x), x\big)\, d\Gamma, \tag{4}$$

where

$$g(u, x) = \sum_{m=1}^{M} \frac{1}{2}\big(u - \hat{u}_m\big)^2 \delta(\|x - x_m\|). \tag{5}$$

Furthermore, the operator (1) may be incorporated as a constraint by defining a new energy

$$\bar{E}_M = \int_\Gamma g\, d\Gamma + \int_\Omega \bar{u}(\mathcal{L}u - S)\, d\Omega, \tag{6}$$

which is equivalent to the original mismatch energy E_M for any test function $\bar{u}$ when the constraint $\mathcal{L}u = S$ is satisfied. Since direct computation of the minimizing boundary surfaces is not possible, we will instead devise a gradient descent procedure in which the change in $\bar{E}_M$ is related to changes in the surface $\Gamma^0 \setminus \Gamma$. This is accomplished by introducing an artificial time dependence $\bar{E}_M(t)$ and carrying out a series of computations to arrive at an expression for $d\bar{E}_M/dt$ in which the sought-after $\partial\Gamma^j/\partial t$ is isolated and can be found in terms of known quantities. In other words, the shape gradient $\partial\Gamma^j/\partial t$ will be expressed in terms of u and $\bar{u}$. These may be computed because each is the solution to a well-posed problem consisting of a governing PDE and appropriate boundary conditions. In general u and $\bar{u}$ would be found numerically, but we present the special case of a spherical inhomogeneity for which a closed-form solution exists.

To carry out the relevant variational calculations, we rewrite $\bar{E}_M$ more directly in terms of the unknown parameters, perform integration by parts, then separate the internal and external boundary integrals as shown in Eq. (7). Note that

$$\begin{aligned}\bar{E}_M &= \int_\Gamma g\, ds + \sum_{j=0}^{n} \int_{\Omega^j} \bar{u}^j(-d^j \triangle u^j + \mu^j u^j - S)\, dx \\ &= \int_\Gamma (g - d^0 B\bar{u}^0 u^0)\, ds + \sum_{j=1}^{n} \int_{\Gamma^j} d^j(\bar{u}^0 - \bar{u}^j)\nabla u^j \cdot N^j\, ds + \sum_{j=0}^{n} \int_{\Omega^j} (d^j \nabla\bar{u}^j \cdot \nabla u^j + \mu^j \bar{u}^j u^j - \bar{u}^j S)\, dx \end{aligned} \tag{7}$$

the boundary conditions (1b) for u are used to simplify the exterior Γ-integral and the flux conditions (2b) for $\mathcal{L}$ are used to simplify the interior Γ^j-integrals. We may then eliminate the interior boundary integrals by imposing the same continuity condition (2a) for the test function $\bar{u}$ as well:

$$\bar{u}^0 = \bar{u}^j, \quad x \in \Gamma^j, \tag{8}$$

leaving us with

$$\begin{aligned}\bar{E}_M = &\int_\Gamma (g + d^0 B\bar{u}u)\, d\Gamma \\ &+ \sum_{j=0}^{n} \int_{\Omega^j} (d^j \nabla\bar{u}\cdot\nabla u + \mu^j \bar{u}u - \bar{u}S)\, d\Omega^j.\end{aligned} \tag{9}$$

C. Shape Sensitivity Analysis

Assuming knowledge of d and μ and an initial guess for $\Gamma^0 \setminus \Gamma$, we wish to determine the variation of $\bar{E}_M$ given a perturbation of the interior boundary Γ^j. We do so by introducing an artificial time variable t and by letting Γ^j be time dependent. As a result, the operator $\mathcal{L}$ will become time dependent and therefore so will u since we continue to impose the constraint (1). Maintaining this constraint allows us to equate the time derivatives of E_M and $\bar{E}_M$ which we relate to the perturbation $\Gamma^j_t = \partial\Gamma^j/\partial t$ of the surface Γ^j (non-integer variables as subscripts will denote partial derivatives with respect to the corresponding variable). Finally, we will make the unknown test function $\bar{u}$ time dependent as well, while continuing to impose the continuity constraint (8). We now proceed by computing the time derivative of our matching energy, shown in (10).

After first applying integration by parts to the volume integrals in (10), the result may be simplified by noting that $\mathcal{L}^j u^j = 0$ and by imposing the following condition on $\bar{u}$:

$$\mathcal{L}^j \bar{u}^j = -d^j \triangle \bar{u}^j + \mu^j \bar{u}^j = 0, \quad x \in \Omega^j, \tag{11}$$

thereby eliminating the volumetric integral terms. The surface Γ^0 is then expanded into its constituent terms, permitting the elimination of the exterior boundary integral (along Γ) by noting the Robin boundary conditions (1b) for u and by choosing the following boundary conditions for $\bar{u}$,

$$d^0\big(B\bar{u} + \frac{\partial\bar{u}}{\partial N}\big) = -g_u, \quad x \in \Gamma. \tag{12}$$

Imposing (12) and replacing u^0 and $\bar{u}^0$ with u^j and $\bar{u}^j$ respectively (as well as substituing $N^0 = -N^j$) yields (13).

To continue the calculation, we need the relationship between u^0_t and u^j_t along the moving boundary $\Gamma^j(t)$, which we obtain by differentiating the continuity conditions (2b) for u and (8) for $\bar{u}$, as shown in (14). Plugging these derivatives into (13) gives an expression that can be further simplified by utlizing the flux condition (2b) for u and by imposing the same condition as our final constraint on $\bar{u}$,

$$d^0 \frac{\partial\bar{u}^0}{\partial N^0} = -d^j \frac{\partial\bar{u}^j}{\partial N^j}, \quad x \in \Gamma^j, \tag{15}$$

finally obtaining (16).

D. Adjoint to the Forward Model

Note that the constraints (8) and (15) on $\bar{u}$ along the internal contours Γ^j, $j = 1, \ldots, n$ are identical to the constraints (2b) connected with our original operator $\mathcal{L}$ and that the local operators $\mathcal{L}^j$ applied to $\bar{u}^j$ over each region Ω^j in the PDE constraint (11) are also identical to those (2a) used by our original operator $\mathcal{L}$. As a result, the overall composite operator used on $\bar{u}$ is the same composite operator $\mathcal{L}$ defined in (2)

$$\begin{aligned}\frac{d\bar{E}_M}{dt} = &\int_\Gamma \big(g_u u_t + d^0 B(\bar{u}_t u + \bar{u}u_t)\big)\, ds + \sum_{j=0}^{n} \int_{\Gamma^j} (d^j \nabla\bar{u}^j\cdot\nabla u^j + \mu^j \bar{u}^j u^j - \bar{u}^j S)(\Gamma^j_t\cdot N^j)\, ds \\ &+ \sum_{j=0}^{n} \int_{\Omega^j} \Big((d^j \nabla\bar{u}^j_t\cdot\nabla u^j + \mu^j \bar{u}^j_t u^j - \bar{u}^j_t S) + (d^j\nabla\bar{u}^j\cdot\nabla u^j_t + \mu^j\bar{u}^j u^j_t)\Big)\, dx\end{aligned} \tag{10}$$

$$\begin{aligned}\frac{d\bar{E}_M}{dt} = &\sum_{i=1}^{n} \int_{\Gamma^j} \Big((d^j\nabla\bar{u}^j\cdot\nabla u^j - d^0\nabla\bar{u}^0\cdot\nabla u^0) + (\mu^j - \mu^0)\bar{u}^j u^j\Big)(\Gamma^j_t\cdot N^j)\, ds \\ &+ \sum_{i=1}^{n} \int_{\Gamma^j} \left(d^0\Big(\bar{u}^0_t \frac{\partial u^0}{\partial N^0} + \frac{\partial\bar{u}^0}{\partial N^0} u^0_t\Big) + d^j\Big(\bar{u}^j_t \frac{\partial u^j}{\partial N^j} + \frac{\partial\bar{u}^j}{\partial N^j} u^j_t\Big)\right) ds\end{aligned} \tag{13}$$

$$\frac{d}{dt}\Big(u^0\big(\Gamma^j(t),t\big) = u^j\big(\Gamma^j(t),t\big)\Big) \quad \longrightarrow \quad u^0_t = u^j_t + (\nabla u^j - \nabla u^0)\cdot\Gamma^j_t = u^j_t + \left(\frac{\partial u^j}{\partial N^j} - \frac{\partial u^0}{\partial N^j}\right)(\Gamma^j_t\cdot N^j) \tag{14}$$

$$\begin{aligned}\frac{d\bar{E}_M}{dt} = &\sum_{j=1}^{n} \int_{\Gamma^j} \Big((d^j\nabla\bar{u}^j\cdot\nabla u^j - d^0\nabla\bar{u}^0\cdot\nabla u^0) + (\mu^j - \mu^0)\bar{u}^j u^j\Big)(\Gamma^j_t\cdot N^j)\, ds \\ &+ \sum_{j=1}^{n} \int_{\Gamma^j} \left(-\left(\frac{\partial\bar{u}^j}{\partial N^j} + \frac{\partial\bar{u}^0}{\partial N^0}\right) d^j \frac{\partial u^j}{\partial N^j} + \left(\frac{\partial u^j}{\partial N^j} + \frac{\partial u^0}{\partial N^0}\right) d^0 \frac{\partial\bar{u}^0}{\partial N^0}\right)(\Gamma^j_t\cdot N^j)\, ds\end{aligned} \tag{16}$$

for u. Thus, together with the boundary conditions (12), the constraints (8), (11), and (15) constitute a well posed problem for $\bar{u}$, allowing us to compute a unique solution. We may thus state the model for $\bar{u}$, the adjoint of u, more compactly:

$$\mathcal{L}\bar{u} = 0, \quad x \in \Omega$$
$$d^0\left(\frac{\partial \bar{u}}{\partial N} + B\bar{u}\right) + \sum_{m=1}^{M}(u - \hat{u}_m)\delta\big(||x - x_m||\big) = 0, \quad x \in \Gamma. \tag{17}$$

E. Shape Gradient

We now complete our shape sensitivity calculation by recognizing that (16) is in the form of a directional derivative: It gives us the the rate of change of $\bar{E}_M$ in terms of the rate of change of the surface Γ^j. The quantity $d\bar{E}_M/dt$ is maximized if Γ^j_t is set equal to the remaining terms on the right-hand side of (16). Thus, the energy is minimized by moving Γ^j in the *opposite* direction. The the shape gradient for an arbitrary 3D surface boundary Γ^j is therefore given by (18).

III. Eigenexpansion of Scattering from a Spherical Inclusion

Since the inclusion is assumed to be spherical, the solution to both the forward (2) and adjoint (17) models can be found using spherical harmonics. For example, from Chapter 16 of [4], we have the following eigenfunction expansion for the solution of (2):

$$\begin{aligned} u^0(r,\phi,\theta) &= G^0(R) + \sum_{n=0}^{\infty}\sum_{m=0}^{\infty} Y_n^m(\phi,\theta) \\ &\quad \cdot \Big[A_{mn}h_n^{(1)}(\mu_0 r) + B_{mn}h_n^{(2)}(\mu_0 r)\Big] \\ u^j(r,\phi,\theta) &= \sum_{n=0}^{\infty}\sum_{m=0}^{\infty} C_{mn}Y_n^m(\phi,\theta)j_n(\mu_j r), \end{aligned} \tag{19}$$

where $k_0 = \sqrt{-\mu^0/d^0}$, $k_j = \sqrt{-\mu^j/d^j}$, and $h_n^{(1)}(\mu_0 r)$ and $h_n^{(2)}(\mu_0 r)$ are the spherical Hankel functions given by combining the Bessel functions of the first and second kinds as shown in Table III. The pair of Hankel functions represents outward $(+)$ and inward $(-)$ propagating waves in a way that is directly analogous to the more familiar representation of free space spherical waves, $\exp\{\pm ikR\}/R$ corresponding to harmonic oscillations of temporal frequency ω, with wavenumber $k = \omega/c$. The terms $Y_n^m(\phi,\theta)$ are spherical harmonics given by:

$$Y_n^m(\phi,\theta) = \sqrt{\frac{(2m+1)}{4\pi}\frac{(n-m)!}{(n+m)!}}\exp\{im\phi\}P_n^m(\theta) \tag{20}$$

where $P_n^m(\theta)$ are the Legendre functions.

The free-space Green's function $G^0(R)$ appearing in Eq. (19) is a function of R, the distance between the source and the point of observation. The remaining terms in (19) and (19) depend on r, ϕ and θ, which are the spherical coordinates representing radius from the origin, azimuth angle, and colatitude (or zenith angle). It is thus useful to expand $G^0(R)$ in terms of these variables using the spherical Bessel functions and Legendre polymonials (i.e., the Legendre functions $P_n^m(\theta)$ for which $m = 0$),

$$\begin{aligned} G^0(R) &= \frac{S}{4\pi d^0}\frac{e^{ik_0 R}}{R} \\ &= \frac{iSk_0}{4\pi d^0}\sum_{n=0}^{\infty}(2n+1)j_n(k_0 r)h_n^{(1)}(k_0\rho)P_n(\theta). \end{aligned} \tag{21}$$

This expansion replaces the dependence on R with dependence on r,ρ, and θ, thus matching quantities used in the other terms in (19) and (19). The variable ρ is new, but known: It represents the distance from the source S to the origin, which is located at the center of the inclusion. The geometry is illustrated in Fig. III.

The outer domain is assumed to be free space. Thus, Γ is considered to be infinitely far away from the source S. In this case, the solution u satisfies the radiation condition, also called the Sommerfeld radiation condition. Quoting Sommerfeld [5]:

> "...the sources must be sources, not sinks of energy. The energy which is radiated from the sources must scatter to infinity; no energy may be radiated from

TABLE I
Spherical Hankel function defined in terms of ordinary Bessel functions of the first and second kinds.

Bessel function of the first kind:	$J_n(x)$
Bessel function of the second kind:	$N_n(x)$
Sph. Bessel function of the first kind:	$j_n(x) = \frac{1}{\sqrt{x}}J_{n+\frac{1}{2}}(x)$
Sph. Bessel function of the second kind:	$n_n(x) = \frac{1}{\sqrt{x}}N_{n+\frac{1}{2}}(x)$
Hankel function of the first kind:	$h_n^{(1)}(x) = j_n(x) + in_n(x)$
Hankel function of the second kind:	$h_n^{(2)}(x) = j_n(x) - in_n(x)$

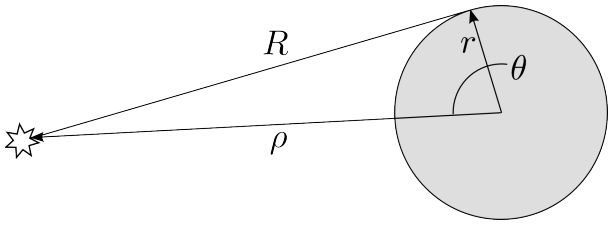

Fig. 2. Coordinates used for the spherical harmonic expansion of u and $\bar{u}$. The distance from the source to a point on the surface of Γ^j is R, while ρ is the distance from center of Γ^j to the source, and θ is the colatitude, or zenith angle. The latitude, or azimuth angle, is not shown but is measured about the axis labeled ρ.

$$\frac{\partial \Gamma^j}{\partial t} = \int_{\Gamma^j}\left[\left(\frac{\partial \bar{u}^j}{\partial N^j} + \frac{\partial \bar{u}^0}{\partial N^0}\right)d^j\frac{\partial u^j}{\partial N^j} - \left(\frac{\partial u^j}{\partial N^j} + \frac{\partial u^0}{\partial N^0}\right)d^0\frac{\partial \bar{u}^0}{\partial N^0} + (d^0\nabla\bar{u}^0\cdot\nabla u^0 - d^j\nabla\bar{u}^j\cdot\nabla u^j) + (\mu^0 - \mu^j)\bar{u}^j u^j\right]N^j\,ds \tag{18}$$

infinity into... the field."

According to the radiation condition, the unbounded outer domain precludes the propagation of any inward-travelling waves. Consequently, the coefficients B_{mn} are all equal to zero since only the outward propagating solution is allowed. Furthermore, the scalar field u and its normal derivative must be continuous at the surface of the spherical inclusion:

$$u^0 = u^j, \quad \text{and} \quad d^0 \frac{\partial u^0}{\partial n^0} = -d^j \frac{\partial u^j}{\partial n^j} \quad \text{on } \Gamma. \tag{22}$$

Since Γ^j is a sphere, the outward normal derivative is simply $\partial/\partial n^j = \partial/\partial r$.

Since the problem is simplified by restricting Ω^j to be a sphere, the resulting configuration is axisymmetric, causing the dependence on the azimuth angle ϕ to vanish. The axis of symmetry is the line of length ρ connecting the source to the center of the spherical flaw as shown in Fig. III.

Simplifying the expansions above and substituting them into the matching boundary conditions gives, for each term in the expansion:

$$\begin{aligned} \frac{ik_0 S}{d^0}\sqrt{\frac{2n+1}{4\pi}} j_n(k_0 r^j) h_n^{(1)}(k_0\rho) + A_n h_n^{(1)}(k_0 r^j) \\ = C_n j_n(k_j r^j) \end{aligned} \tag{23}$$

$$\begin{aligned} ik_0^2 S\sqrt{\frac{2n+1}{4\pi}} j_n'(k_0 r^j) h_n^{(1)}(k_0\rho) + A_n d^0 k_0 h_n'^{(1)}(k_0 r^j) \\ = C_n d^j k_j j_n'(k_j r^j). \end{aligned} \tag{24}$$

Due to axisymmetry, the only nonzero values of the expansion coefficients correspond to the index $m = 0$, since the exponential function and Legendre function within the spherical harmonics (20) are constant for all azimuth angles only when $m = 0$. For notational simplicity, the m index is suppressed (i.e., A_{0n} is written as A_n).

The pair of equations above can be arranged into a 2×2 system of linear equations, which can be easily solved for the coefficients for a single term in the expansion:

$$\begin{aligned} &\begin{bmatrix} -h_n^{(1)}(k_0 r^j) & j_n(k_j r^j) \\ -k_0 d^0 h_n'^{(1)}(k_0 r^j) & d^j k_j j_n'(k_j r^j) \end{bmatrix} \begin{bmatrix} A_n \\ C_n \end{bmatrix} \\ &= \frac{ik_0 S}{d^0}\sqrt{\frac{2n+1}{4\pi}} h_n^{(1)}(k_0\rho) \begin{bmatrix} j_n(k_0 r^j) \\ k_0 d^0 j_n'(k_0 r^j) \end{bmatrix}. \end{aligned} \tag{25}$$

The derivative terms can be computed according to the recursion [6],

$$f_n'(x) = \frac{n}{x} f_n(x) - f_{n+1}(x),$$

and the 2×2 system can be solved explicitly for A_n and C_n.

Given the source strength and position, along with the position and radius of the sphere Ω^j, the scattered field is given in closed form by summing over the terms in the harmonic expansion.

Computing the value of Γ_t^j for a spherical flaw embedded in free space requires knowledge of the fields u and $\bar{u}$ both inside and outside the sphere. Equation (25) is used to compute u^0 and u^j. It also serves as a prototype for computing the adjoint field $\bar{u}$:

$$\begin{aligned} &\begin{bmatrix} -h_n^{(2)}(k_0 r^j) & j_n(k_j r^j) \\ -k_0 h_n'^{(2)}(k_0 r^j) & -d^j k_j j_n'(k_j r^j) \end{bmatrix} \begin{bmatrix} \bar{A}_n \\ \bar{C}_n \end{bmatrix} \\ &= \frac{-ik_0 S_M}{d^0}\sqrt{\frac{2n+1}{4\pi}} h_n^{(2)}(k_0\rho) \begin{bmatrix} j_n(k_0 r^j) \\ d^0 j_n'(k_0 r^j) \end{bmatrix} \end{aligned} \tag{26}$$

in which the measurement errors $S_m = \hat{u}_m(x_m) - u(x_m)$ act as source terms replacing S in (25).

It is important to note that the forward and adjoint fields generally have different axes of symmetry since the vectors from the center of Ω^j to the respective sources are different. It is therefore necessary to transform from the natural 'local' spherical coordinates into a common frame of reference when computing the required scalar fields and their gradients. This is conveniently done using twist coordinates.

IV. Gradient descent approach

The position x_{sph} and radius r_{sph} of the spherical inclusion embedded in free space are unknown. Its location can be found iteratively via gradient descent. These parameters are assumed at each step and are used to model the scattered field, which is compared with the observed measurements. This mismatch provides the source terms used in the adjoint formulation that backpropagates the adjoint field to the surface of the current guess Γ^j. The forward-modeled and adjoint fields are used to find the change in the summed squared error that would result from a given perturbation of the flaw position and radius, as described in Section III. The general algorithm is as follows:

Make an initial guess of the sphere's position and radius.
while Stopping condition is not satisfied **do**
  Compute Γ_t^j based on
    current values of x_{sph}, r_{sph}, $\bar{u}$, and u.
  Update x_{sph} and r_{sph}.
  Compute updated $\bar{u}$ and u.
end while

The stopping condition is reached when the norm of Γ_t^j falls below some specified threshold.

The results from the two previous sections are used to construct the solution for finding the position and radius of a spherical flaw embedded in a homogeneous medium. The general result (18) is used, and Γ^j is constrained to be a sphere for which only the radius r_{sph} and location x_{sph} may be altered by the gradient descent flow. Only a single sphere is considered, so $j = 1$. The constraints are imposed by integrating over the surface Γ^j the inner product of Γ_t^j with appropriate vectors. The rate of radial expansion dr_{sph}/dt is found by integrating the inner product of Γ_t^j and the unit vector N^j normal to Γ^j. The movement dx_{sph}/dt of Γ^j in each of the directions e_1, e_2, and e_3 is given by simply integrating $\Gamma_t^j \cdot e_i$ over the surface Γ^j.

The field u and its adjoint can be computed easily by solving (25) and (26) for all the terms one wishes to include in the

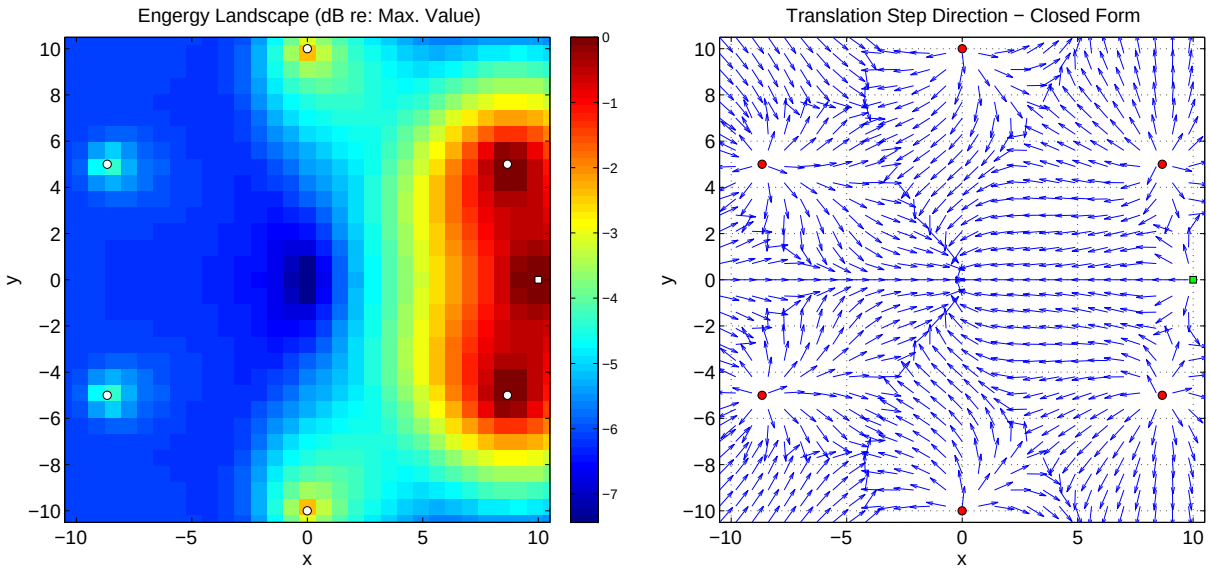

(a) Energy landscape (b) Closed form

Fig. 3. Left: Source (square) and measurements (circles) configured in a ring. Right: Energy g computed for a region of the (x, y) plane: $x \in [-10.5\ 10.5]$ and $y \in [-10.5\ 10.5]$. The plot is shown in terms of decibels relative to the peak value of the energy in the computed region. The gradient of this energy landscape drives the position of the active surface toward the true value, so long as the initial guess is within the ring of measurements.

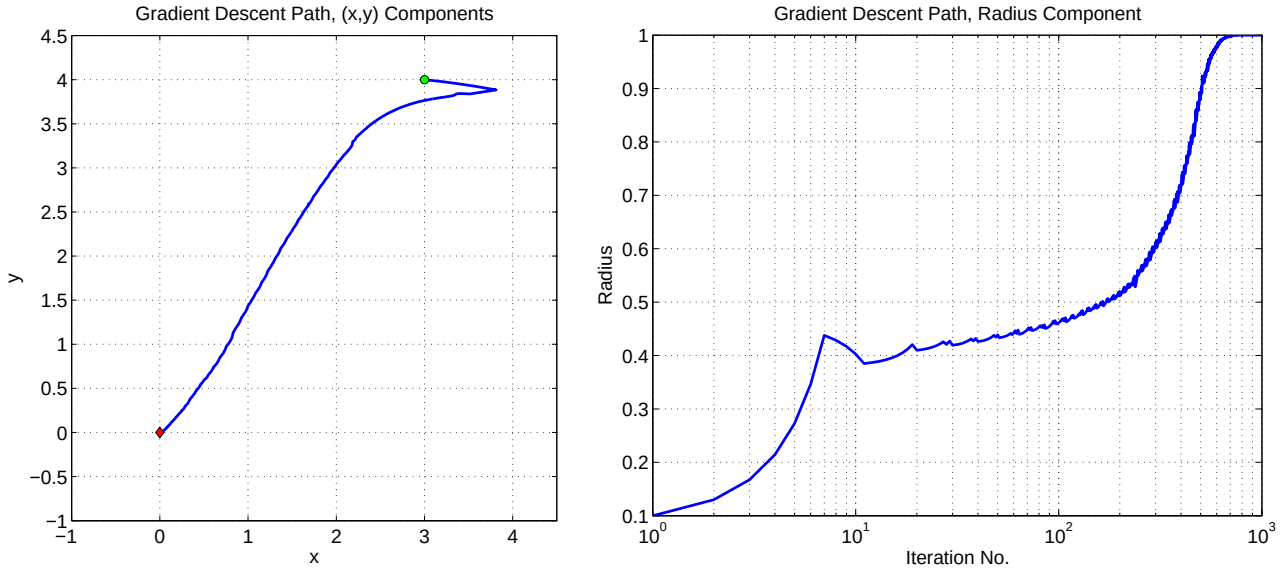

(a) Descent path (b) Radius

Fig. 4. Path (left) and corresponding radius (right) as the gradient descent algorithm reduces the energy $\bar{E}_M$. The start and end of the gradient descent path are indicated by the green circle and red diamond, respectively.

expansion. The gradient terms appearing in (18) can be found in closed form using properties of spherical harmonics.

V. Results and Discussion

As stated previously, we are interested in using active surfaces to determine the radius and position of an unknown sphere, or inclusion, located within a medium. The material properties of the medium and the inclusion are known. Measurements of single-frequency (i.e., monochromatic) scattered waves are made in a region surrounding the location of the inclusion.

The example shown in Fig. 3 consists of a single source and a ring of six measurement positions. The source is at the same radius (10 units) as the measurements.

The material properties used for this example are $d^0 = d^i = 1$, $\mu^0 = 0.1$, and $\mu^i = 0.01$. These values cause Eq. (2) to describe a lossy medium since the wavenumbers are purely imaginary. The spherical inclusion and the surrounding medium are diffusive, as might be the case for the detection of tumors within the body using fluorescence tomography [7]. Recall that the energy g is given by the summed-squared difference between the true field and the computed field based on the current guess of the sphere's position and radius.

For this example, the true sphere has unit radius and is located at the origin. An energy landscape can be visualized by marching the current guess of the sphere's position over a rectangular grid spanning the region of interest, as in Fig. 3. The summed squared difference between the measured and predicted scattered field is displayed for each point. As expected, the minimum energy occurs at the origin. Although it is not shown, performing this same computation using the incorrect radius can cause the minimum to shift away from the true position of the inclusion. Such effects must be considered when devising the gradient descent scheme to be implemented.

Figure 4 shows a gradient descent for which the initial guess position is $(x, y) = (3, 4)$, and for which the radius is initially supposed to be 10 times too small ($r = 0.1$). The solution converges, making several pauses along the way as the radius updates. This is an artifact of the gradient descent procedure used. In this example the direction of the gradient descent step is given by the closed-form computation, and the step size is controlled by the user. Starting from a specified initial value, the step size is increased at each iteration as long as the energy decreases. If a step results in an increase in $\bar{E}_M$, then the step size is cut dramatically, and the gradient descent changes direction significantly. This scheme results in overshoot and is responsible for the zig-zag pattern and the irregular step sizes observed.

A. Extension to Acoustics and Buried Objects

The methodology presented above can be applied to underwater acoustics and extended to the two-medium problem of locating a spherical inclusion within one medium using sources and observations in a second, as shown in Fig. 5. The diffusive model (2) derived above can be transformed into the familiar lossless Helmholtz equation by setting $d^0 = d^j = -1$. Furthermore, we model the water and sediment as a pair of fluid half spaces, which is a reasonable approximation under certain conditions [8]. The sediment is represented by a fluid so that the governing acoustic equation does not change, and only boundary conditions need to be matched. In more complicated sediments one would need to consider coupling between the water and modes of propagation supported by solids.

As before, we use spherical harmonics to represent the total acoustic pressure field, noting that boundary conditions must now be matched at the interface as well as on the surface of the inclusion in Medium 2. The field in Medium 1 consists of the source field, its reflection from the interface, and the scattered contribution from the inclusion in Medium 2. The field in Medium 2 consists of the transmitted source field, the field scattered by the inclusion, and the reflection of the scattered field from the interface. The reflected fields are modeled using the method of images. The interior of the inclusion is not modeled, on the grounds that it is assumed to be acoustically soft or hard. These are limiting conditions implying either Neumann or Dirichlet boundary conditions, respectively. Thus, there are a total of six fields to be considered, compared to two used in Section III.

A closed-form solution to the two-fluid problem should be achievable, albeit far more challenging to accomplish due to the added complexity that comes from having to consider four additional fields. Furthermore, the problem is not axisymmetric so the spherical harmonics Y_n^m are no longer equal to zero for $m > 0$. Because of this anticipated complexity, we consider the alternative approach of numerically solving for the total acoustic field. One suitable approach would be to use the collocation method to discretize the interface using N points. Applying the boundary conditions at these points leads to a system of $2N$ linear equations which can be solved for the N coefficients required to describe the acoustic field on each side of the interface. This procedure would be repeated for the adjoint field required by each of the M measurement points.

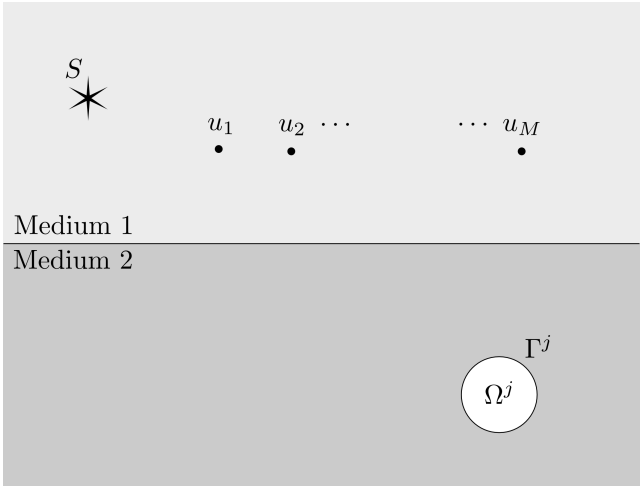

Fig. 5. Source illuminating a two-fluid configuration in which the inclusion resides in one fluid and the source/measurements reside in the other. A single source is shown from clarity. The technique presented is equally valid for an arbitrary number of sources.

This problem could be extended even further to consider the effects of shallow water. In this case, the water column would not be a half space. Rather, it would feature a pressure-release (perfectly reflecting) boundary condition. As with the water/sediment interface, the surface effects can be modeled using the method of images. An interesting consequence of including sea surface effects is that the multipath environment might actually work to our advantage, as the image sources could provide spatial diversity having the same net effect as using additional sources.

VI. Conclusion

We have presented the foundational aspects of a new image reconstruction approach for a broad range of problems where the information sought is a representation of boundaries rather than a pixel-by-pixel map of a region of interest. The method derived in Section II is completely general, applying to any set of simply-connected inhomogeneities. This result was constrained in Section III to the case of a single spherical inclusion in order to demonstrate the gradient descent procedure used to find the boundary surfaces of interest. More complicated geometries and applications, such as searching for objects buried in the sea floor, will require numerical solutions for

the forward and adjoint fields necessary to compute the shape derivative used to drive the active surface. These are the subject of ongoing research.

REFERENCES

[1] A. Kumar, A. Yezzi, S. Kichenassamy, P. Olver, and A. Tannenbaum, "Active contours for visual tracking: A geometric gradient based approach," *Proceedings of IEEE Conference on Decision and Control*, vol. 4, pp. 4041–4046, December 1995.

[2] O. Faugeras and R. Keriven, "Variational principles, surface evolution, pdes, level set methods and the stereo problem," *IEEE Transactions on Image Processing*, vol. 7, no. 3, pp. 336–344, 1998.

[3] G. Sundaramoorthi, J. Jackson, A. Yezzi, and A. Mennucci, "Tracking with Sobolev active countors," *Proceedings of Computer Vision and Pattern Recognition*, vol. 1, pp. 674–680, June 2006.

[4] J. D. Jackson, *Classical Electrodynamics*. John Wiley and Sons, 1975.

[5] A. Sommerfeld, *Partial Differential Equations in Physics*. New York, New York: Academic Press, 1949.

[6] "NIST Digital Library of Mathematical Functions, NIST-DLMF," `http://dlmf.nist.gov`.

[7] F. Fedele, M. J. Eppstein, J. P. Laible, A. Godavarty, and E. M. Sevick-Muraca, "Fluorescence photon migration by the boundary element method," *Journal of Computational Physics*, vol. 210, pp. 109–132, 2010.

[8] C. S. Clay and H. Medwin, *Acoustical Oceanography*. John Wiley and Sons, Inc., 1977.